Analysis of nonlinear wavelength conversion system for a red–green–blue laser-projection source

Edith Innerhofer, Felix Brunner, Sergio V. Marchese, and Rüdiger Paschotta

ETH Zürich, Physics Department, Institute of Quantum Electronics, Wolfgang-Pauli-Str. 16, CH-8093 Zürich, Switzerland

Gunnar Arisholm

Forsvarets Forskningsinstitutt FFI (Norwegian Defence Research Establishment), Postboks 25, NO–2027 Kjeller, Norway

Sunao Kurimura and Kenji Kitamura

National Institute for Materials Science, Namiki 1-1, Tsukuba 305–0044, Japan

Takeshi Usami and Hiromasa Ito

Research Institute of Electrical Communication RIEC, Tohoku University, Katahira 2-1-1, Aobaku, Sendai 980–8577, Japan

Ursula Keller

ETH Zürich, Physics Department, Institute of Quantum Electronics, Wolfgang-Pauli-Str. 16, CH–8093 Zürich, Switzerland

Received May 27, 2005; revised September 16, 2005; accepted September 16, 2005

We analyze the physical processes in the nonlinear wavelength conversion stages of a recently demonstrated red–green–blue (RGB) laser source, which generated ⩾8 W of average power in each color. The system is based on an infrared femtosecond mode-locked laser and contains a frequency doubler, a parametric generator, a parametric amplifier, and two sum-frequency conversion stages. It does not require any resonant cavities, external laser amplifiers, or nonlinear crystals operated at elevated temperatures; therefore it appears to be more practical than other previously demonstrated RGB laser sources. However, the optimization of the overall system is nontrivial, because pump depletion, birefringence, and temporal walk-off in the first conversion stages lead to spatial and temporal distortion of the interacting beams in the subsequent nonlinear conversion stages. This leads to the interaction of spatially and temporally distorted beams in the later conversion stages. By using a numerical simulation of the nonlinear conversion processes based on a Fourier-space method in one temporal and two transverse spatial dimensions, we can fully take into account these effects. We analyze and discuss the physical effects in the different conversion stages and describe the optimization of the overall system performance.

OCIS codes: 140.4050, 190.7110.

1. INTRODUCTION

There is a demand for digital laser-projection displays, sufficiently large to be used, e.g., in cinemas and for flight simulators. Laser projectors have numerous advantages over conventional lamp projectors. The color gamut from a red–green–blue (RGB) laser source is much wider than that from a high-definition TV, and excellent color saturation can be achieved. Additional advantages of an RGB projector compared to analog film rolls include fully digital data recording, handling, transmission, and storage. Moreover, the large focal depth of a laser beam even allows for projection onto curved surfaces.

The required projection technology already exists; an example is the grating light valve projector.[1,2] The major challenge is the design of a suitable RGB laser source with high output power of ≈10 W per color, particularly when additional features such as long lifetime, stable maintenance-free long-term operation, compactness, and reasonable price are required. An interesting approach is to start with a single infrared laser, from which all colors are generated in nonlinear conversion stages. Previously, the required high infrared power for a system with several watts per color could be produced only by supplementing the infrared laser with one or more amplifier stages.[3,4] The introduction of the passively mode-locked thin disk laser,[5–7] which allows generation of very high (several tens of watts) powers directly, promises a significant advance toward commercially viable RGB sources.

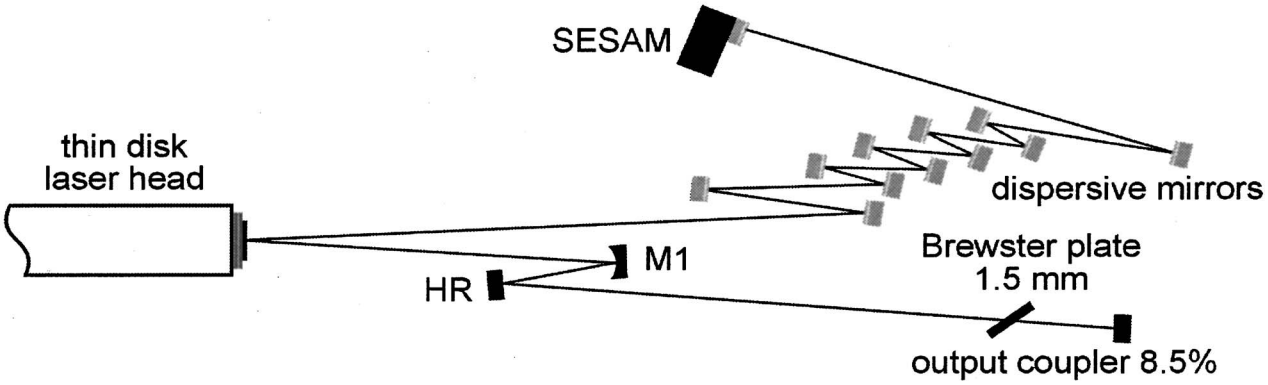

Fig. 1. Setup of the Yb:YAG thin disk laser for the 780 fs pulses. M1, spherically curved mirror; HR, high reflective mirror; SESAM, semiconductor saturable absorber mirror.

For a given laser wavelength, a variety of different combinations of nonlinear conversion stages could generate the RGB beams (see Ref. 8). In practice, the viability of a scheme depends strongly on other laser parameters, such as pulse duration, peak power, and beam quality. Ideally, one should find the optimal conversion scheme for given laser parameters. However, this would be prohibitively complicated because of the number of possible schemes to be evaluated and the large number of parameters corresponding to multiple conversion stages in each scheme. Furthermore, there is no well-defined optimum in terms of technical parameters, like output power and beam quality. The optimal scheme in an application may depend on additional constraints, such as cost and availability of components. For these reasons we restrict our analysis to one particular scheme, which we have recently demonstrated.[9] Important design parameters of such a system are phase-matching schemes, crystal lengths, and focusing parameters, which we optimized using numerical methods.[10] The RGB system consists of a passively mode-locked thin disk laser, a frequency doubler, an optical parametric generator (OPG), an optical parametric amplifier (OPA), and two sum frequency generation (SFG) stages. Compared with Ref. 9, we analyze in detail the approach based on an OPG and an OPA for the generation of beams at 800 nm and at 1.5 μm. This makes the advantages of such an RGB system even more apparent. Thanks to the short pulses and high peak power that a mode-locked thin disk laser generates, we do not need resonant conversion stages, and with the exception of the OPG, all of the crystals are critically phase matched and operated at room temperature. The now temperature-stabilized crystal in the OPG stage can be replaced with a magnesium-doped crystal operated at room temperature, as we have recently shown.[11] Our analysis of the RGB system is based both on the mentioned experimental results and on an advanced numerical model[10] that allows the simulation of the nonlinear conversion processes.

This article is organized as follows. In Section 2, we describe in more detail (compared with Ref. 9) the experimental setup of the Yb:YAG thin disk laser, which delivers a record-high average power of nearly 80 W in 780 fs pulses. In Section 3, we discuss the experimental and simulation results for the second-harmonic-generation stage. The advantages of a setup with an OPG and a subsequent OPA and its performance details are addressed in Section 4. The two SFG stages are discussed in Section 5. Finally, Section 6 presents a discussion of the overall system and its potential for further improvements.

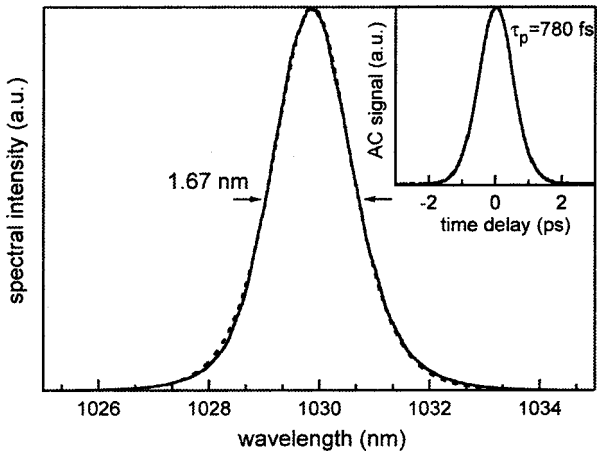

Fig. 2. Measured optical spectrum and autocorrelation trace (inset) of the 780 fs pulses obtained from the thin disk Yb:YAG laser at 79 W average output power. The dashed curves, representing sech^2 fits, overlap the data well.

2. Yb:YAG THIN DISK LASER

The infrared pump power for the nonlinear conversion stages of our RGB system is delivered by an Yb:YAG thin disk laser[12] that is passively mode locked with a semiconductor saturable absorber mirror (SESAM).[13,14] This laser is a modified version of the laser described in Ref. 6, with higher average output power and higher pulse repetition rate. Figure 1 shows the cavity setup. The required group delay dispersion (GDD) for soliton mode locking[15,16] is introduced by 11 Gires–Tournois interferometer-type dispersive mirrors,[17] generating a total GDD of -12100 fs^2 per round trip. The 1.5 mm thick Brewster plate is used to increase the Kerr nonlinearity and to enforce a linear laser polarization. We obtain self-starting stable mode locking with an average output power of 79 W (with a pump power of 360 W) in pulses of 780 fs duration at a center wavelength of 1030 nm (Fig. 2). The transmission of the output coupler is 8.5%. The pulse repetition rate is 57 MHz, leading to an output pulse energy of 1.39 μJ and a peak power as high as 1.57 MW. With a spectral bandwidth of 1.67 nm, the time-bandwidth product is 0.37,

which is slightly larger than the ideal time-bandwidth product for soliton pulses (0.315). All pulse lengths and spectral widths are given as FWHM and the time-bandwidth products are based on these measures.

3. SECOND-HARMONIC GENERATION

The first nonlinear conversion stage in the RGB system is a second-harmonic generator, which converts part of the fundamental 1030 nm light into green light at 515 nm. As the green wave first serves as pump for the OPA and then the residual light is used for the display, a high power is important. In addition, because the residual 1030 nm light is used as pump wave for further conversion stages, it is essential to retain a good beam quality as well as sufficient power in this beam, too.

A. Experiment

The second harmonic is generated in a 5 mm long antireflection-coated LiB_3O_5 (LBO) crystal, as shown in Fig. 3. LBO is an attractive nonlinear material with versatile phase-matching options and the potential for high-power operation. We use a critical phase-matching scheme of Type I (oo-e) at room temperature with a phase-matching angle of $\varphi_{pm}=13.77°$ and a nonlinear coefficient of $d_{31}=0.85$ pm/V[18,19] (using the notation of Roberts[20]). For the phase-matching scheme with the propagation direction in the XY plane, the effective nonlinearity is $d_{eff}=d_{31}\cos(\varphi_{pm})=0.827$ pm/V, and the walk-off angle for the second-harmonic wave is $\rho=8.29$ mrad. The pump beam was focused to a spot with a beam waist of ≈ 130 μm radius. If not indicated otherwise, all beam radii correspond to $1/e^2$ intensity radii. With the crystal in the beam waist, we obtained up to 48 W of average power at 515 nm, corresponding to a conversion efficiency of 61%. However, this conversion efficiency is too high for our RGB scheme, which also uses the transmitted fundamental radiation in the following conversion stages. Therefore, during the RGB experiment, we intentionally moved the SHG crystal somewhat out of the beam focus to a position with pump radius ≈ 150 μm so as to obtain 45.6 W in the green beam and 30.3 W residual power at 1030 nm. At this power level, the pump intensity in the LBO crystal was 4.4 GW/cm^2, which still is below the damage threshold of LBO for femtosecond pulse durations. [All other LBO crystals run a lower risk of damage since they are operated with smaller intensities and (mostly) with longer wavelengths.] The beam quality of the green wave is close to the diffraction limit with an M^2 value of 1.1, where a knife-edge method was used for the measurement.

B. Simulation and Discussion

We simulated the nonlinear interaction in the SHG stage using a numerical model. The model has been previously described,[10,21] so we review it only briefly here. Propagation with diffraction is handled by decomposing the beams in monochromatic plane-wave components. By taking into account the direction dependence of the refractive index of the plane-wave components in a birefringent crystal, birefringence effects such as spatial walk-off and anisotropic diffraction are included. With the exception of propagation along the optical axes in biaxial crystals, the model can handle arbitrary propagation directions. Furthermore, by including the wavelength dependence of the

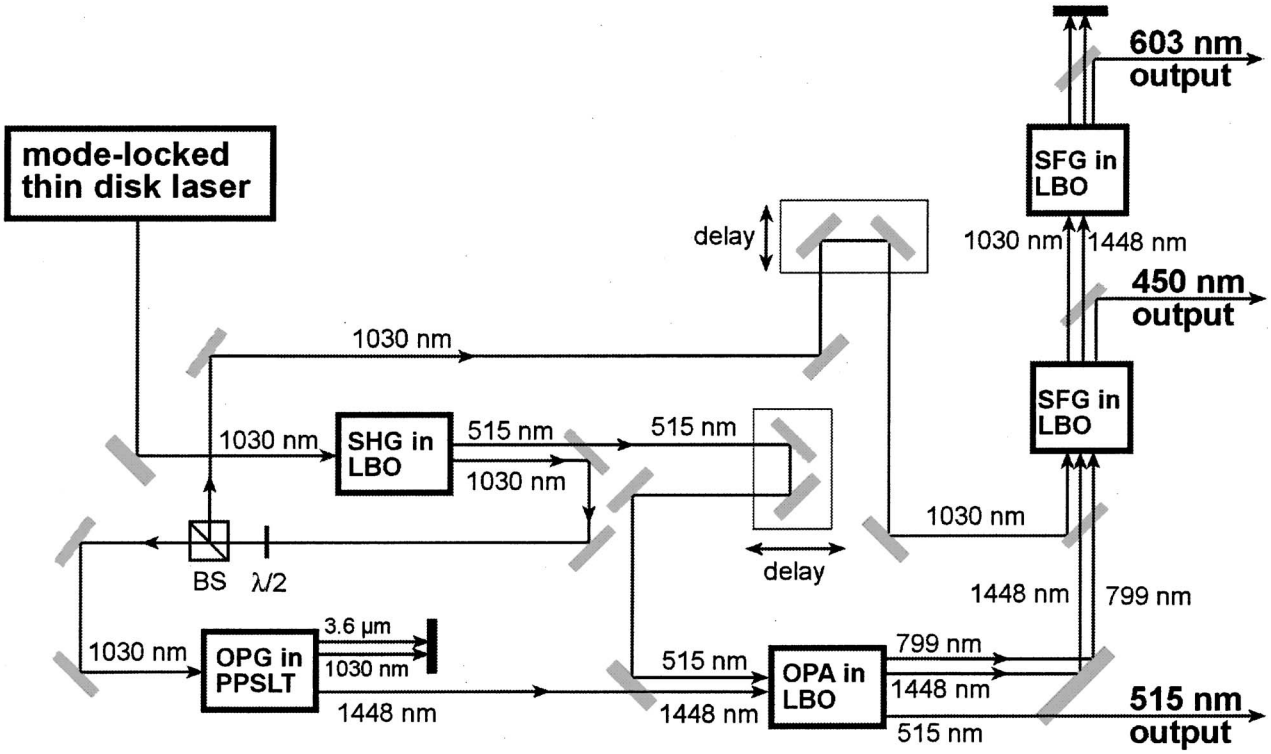

Fig. 3. Experimental setup of the RGB source. BS, beam splitter; SHG, second-harmonic generation; OPG, optical parametric generation; OPA, optical parametric amplification; SFG, sum-frequency generation. All beams are collinear in the nonlinear crystals, although for clarity they are shown with some spatial separation.

refractive index (e.g., by Sellmeier equations), dispersion is also handled exactly. The coupled differential equations for the interacting beams can be solved either directly in spatial and temporal frequency space or by a split-step method. The latter method requires less memory, but in the present work we used the frequency-space method, because we had no problem with memory constraints.

Although the model works with equations for the envelopes, it does not rely on the slowly varying envelope approximation. The program calculates the spatial evolution of the amplitude of each spectral and angular component. The essential approximation is that the spectral amplitudes vary slowly compared with the optical wavelength. Since the rate of change of these amplitudes is determined by the gain coefficient, which is on the order of a few inverse millimeters, this approximation is well satisfied even in high gain OPAs.[22] The absence of the slowly varying envelope approximation, combined with exact dispersion, makes the model suitable even for ultrashort pulses.

To save time and memory, one can instruct the model to take advantage of cylindrical symmetry or the symmetry about the critical plane and compute the beam amplitudes along a radial line or on a single half-plane, respectively. In addition to the core function for propagation in nonlinear crystals, the model includes functions for free-space propagation, various optical components, and beam sources. In particular, the output beams from a simulation can be used as input in the simulation of a subsequent nonlinear conversion stage. This feature is important in the RGB system, because some of the pump beams are used sequentially in multiple stages, and depletion of the beam in one stage affects the performance of subsequent stages.

The numerical simulations are generally in good agreement with the measurements. For example, we measured an average power of 45.6 W at 515 nm after the SHG stage and simulated an average power of 48.5 W, resulting in a deviation of ≈6%. Figure 4 shows beam quality and conversion efficiency for increasing fundamental power. The quality of the generated second-harmonic wave remains good even for very high conversion efficiencies, e.g., the simulation yields $M^2 < 1.1$ even for 84% conversion efficiency. On the other hand, owing to pump depletion, the M^2 factor of the residual pump wave increases for increasing conversion efficiency. In an experimental situation, one would rather increase the crystal length than the pump power in order to avoid crystal damage. Nevertheless, this simulation shows that good beam quality can be obtained with high conversion efficiency. For such a situation, simulations predict that a conversion efficiency of 86% could be obtained by using a longer (12 mm) LBO crystal with the same pump intensity as used for the RGB experiment. While the generated green wave still shows an M^2 factor of 1.04 at a conversion efficiency of 86%, the beam quality of the pump beam has already deteriorated. For the experimental conditions, good beam quality for both the second-harmonic wave and the residual pump is expected. As a result of pump depletion and temporal walk-off, the pulse durations of the second-harmonic wave and the transmitted pump beam increase for increasing conversion efficiency. For the 5 mm long LBO crystal used in the experiment, the spatial walk-off is more important than the temporal walk-off. The amount of generated green power is crucial for the following OPG–OPA stage, as it serves as the pump power for the amplifier stage. At the same time, however, we also need sufficient power at 1030 nm for the OPG and the subsequent sum-frequency stages.

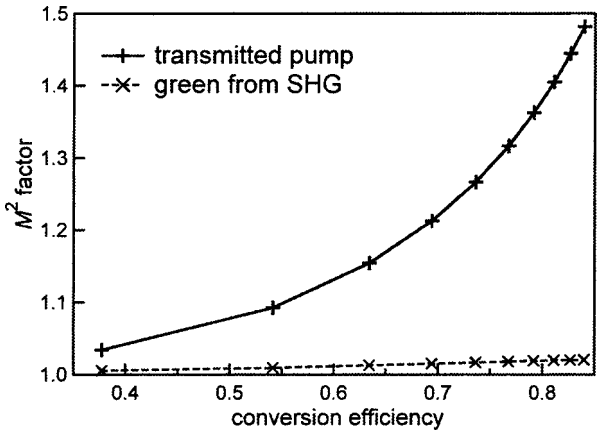

Fig. 4. Simulated beam quality of the second-harmonic wave at 515 nm and of the transmitted pump wave at 1030 nm in the frequency doubler. The data points correspond to different pump powers in the range of 30–300 W, and the beam quality is plotted versus the conversion efficiency. The M^2 factor of the 515 nm wave stays well below 1.1, even for very high conversion efficiencies.

4. OPTICAL PARAMETRIC GENERATOR AND OPTICAL PARAMETRIC AMPLIFIER

We have chosen the approach of an OPG and a subsequent OPA to generate waves with multiwatt average power at 800 nm and at 1.5 μm required for the following SFG stages. As we will show, this approach solves several problems encountered for high power levels.

A. Experiment

The OPG stage generates a seed beam at 1448 nm and an idler beam at 3568 nm and is based on a periodically poled stoichiometric $LiTaO_3$ (PPSLT) crystal.[23] This material is very attractive for high-power parametric processes because of its high nonlinearity and its high photorefractive damage resistance. The OPA stage, based on LBO, boosts the power at 1448 nm to the multiwatt level and at the same time creates an idler wave at 799 nm. The two-stage approach allows for a nearly diffraction-limited beam quality of signal and idler waves, because the power amplifier stage is operated with a lower gain (energy gain of ≈8 dB) so that gain guiding is less important.

We pump the OPG stage with a fraction of the residual 1030 nm light from the SHG. The uncoated PPSLT crystal of the OPG stage has a length of 17.5 mm and a thickness of 1 mm, and the width of the periodically poled region is ≈2.5 mm. In the current system it is operated in a temperature-stabilized oven at 150 °C to avoid photorefractive damage, but recently we have demonstrated stable room-temperature OPG operation in MgO-doped

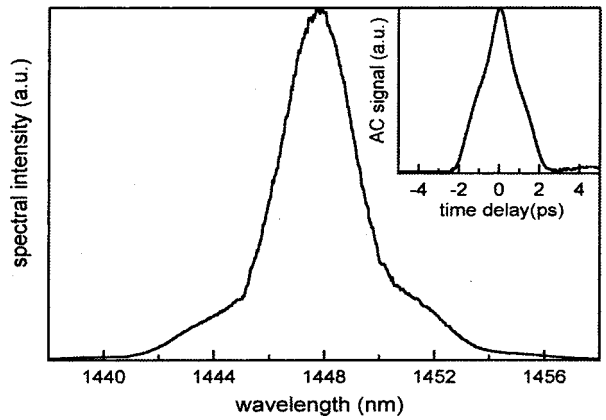

Fig. 5. Measured optical spectrum and autocorrelation trace (inset) from the OPG at 1.6 W of signal average power.

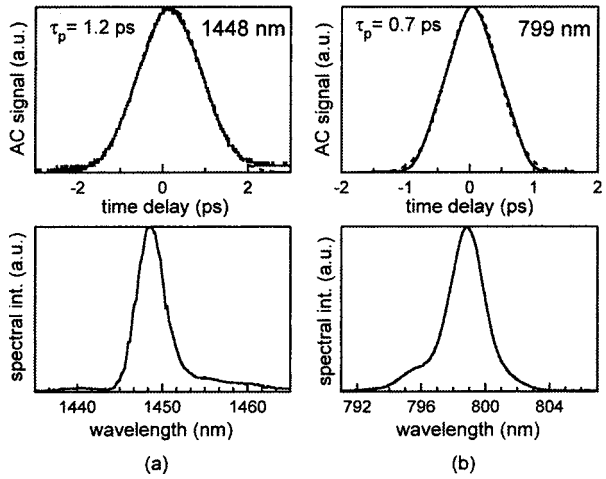

Fig. 6. Measured optical spectrum (bottom) and autocorrelation (top) trace of the signal (a) and idler (b) wave of the OPA.

SLT with high average power,[11] which would allow room-temperature operation in a future RGB system.

The generated wavelengths of the OPG are determined by the poling period and the operation temperature of the crystal. The crystal we use has a poling period of 29 μm, which leads to phase-matched wavelengths of 1448 nm for the signal and 3568 nm for the idler at the operation temperature of 150 °C. Using a reported Sellmeier equation,[24] the dependence of the signal wavelength on temperature is $\approx$0.23 nm/K and on the grating period $\approx$69 nm/μm in our regime of operation. A change of 1 nm in the signal wavelength of the OPG would thus require a change of the crystal temperature by $\approx$4 K. However, this change in the signal wavelength would only lead to a wavelength change of $<$0.2 nm in the red output and $<$0.1 nm in the blue output. We use the PPSLT crystal in a double-pass configuration to obtain sufficient parametric gain without reaching the threshold for optical damage. After a first pass through the crystal, the pump and signal waves are reimaged with a curved mirror into the crystal for a second pass. The idler wave and some parasitic green light arising from higher-order phase-matched second-harmonic generation are eliminated after the first pass through the OPG crystal. Finally, the signal wave is separated from the pump with a dichroic mirror. The nonlinear coefficient of the PPSLT crystal is estimated to be 8.2 pm/V (see Subsection 4.B). Fresnel reflections on the uncoated crystal faces introduce relatively large losses of $\approx$13% per surface, which could be drastically reduced with an antireflection coating. The pump waist in the nonlinear crystal is 22 μm, which leads to an internal pump peak intensity of 11.6 GW/cm^2, calculated with the simulated pump pulse duration of 1180 fs for the residual 1030 nm wave after the SHG stage, for 7.7 W of pump power incident on the crystal. At this intensity, the OPG runs stably without crystal damage and generates 1.6 W of average power at 1448 nm. The OPG threshold was at 6.4 W of pump power incident on the crystal. The measured intensity autocorrelation and the optical spectrum at a signal average power of 1.6 W are shown in Fig. 5. The intensity autocorrelation shows signs of strong temporal pulse distortion (see Subsection 4.B). Despite this temporal pulse distortion, we roughly estimated the FWHM pulse duration of the signal to $\approx$1.4 ps (for a sech^2 fit).

The parametric amplifier stage is based on a 10 mm long LBO crystal that is critically phase matched at room temperature. The LBO crystal in the OPA is pumped with the green beam from the SHG. The beam waist of the 515 nm wave in the antireflection-coated LBO crystal is 125 μm and the signal waist 210 μm. The antireflection coating (AR) of the LBO introduces relatively large reflection losses of 1% at 515 nm, 2% at 799 nm, and 4.2% at 1448 nm, which could be reduced with better coatings. Phase matching is achieved with a Type I scheme (oo-e in the *XY* plane) at room temperature with a phase-matching angle of $\varphi_{pm}=11.85°$ and a nonlinear coefficient of $d_{31}=0.85$ pm/V. The effective nonlinearity is 0.83 pm/V, and the walk-off angle of the pump wave is $\rho=7.21$ mrad. The peak intensity of the pump wave in the LBO crystal for a pump power of 42.4 W is calculated to be 3.9 GW/cm^2, without pump depletion and for a simulated duration of the green pump pulses of 680 fs. We obtained up to 7 W of signal power at 1448 nm and 11.9 W of idler power at 799 nm. The internal conversion efficiency from pump to signal and idler wave combined is 47%. The measured pulse durations for signal and idler are 1.2 and 0.7 ps, respectively (see Fig. 6). The beam quality of the idler is close to the diffraction limit, with a measured M^2 factor of 1.2. The residual 23 W of green light is separated from the signal and idler wavelengths and used as first output of the RGB system. The beam quality of the 515 nm output is still fairly good, with an M^2 factor of 1.9. The degradation of the spatial beam quality of the 515 nm light is caused by pump depletion in the OPA stage.

B. Simulation and Discussion

For the generation of wavelengths in the blue and red spectral regions with the process of SFG with the fundamental wave at 1030 nm, beams at 800 nm and 1.5 μm with high average power and good beam quality are required. Optical parametric oscillators (OPOs) are often used to generate beams in the 1.5 μm spectral region. However, a disadvantage is the required synchronization of the OPO cavity with the laser cavity, which for long-term stable operation in the femtosecond regime often re-

quires a feedback stabilization scheme, would make the RGB setup more complex. Such additional complexity is avoided with the use of an OPG. However, OPGs require a high parametric gain and thus high intensities in the nonlinear crystal. Therefore OPGs are typically pumped with amplified laser sources that operate at kilohertz repetition rates and thus are not suitable for most laser displays. An OPG directly pumped with a mode-locked laser at a multimegahertz repetition rate was demonstrated for the first time in 2001 with femtosecond pulses from a passively mode-locked thin disk laser.[25,26] Somewhat later, similar experiments were performed with higher average power in picosecond pulses.[27]

Although the necessary pump power is now directly available from lasers, the generation of high power 800 nm and 1.5 μm beams in a single OPG stage is not practical. First, it has been recognized that the combination of high parametric gain, high output power and good conversion efficiency is subject to severe limitations that are related to gain guiding.[21] Second, generating these wavelengths in an OPG would require a green pump beam, and crystals with gain high enough for the OPG, such as lithium tantalate, would be susceptible to optical damage from a high-power green beam. By combining a 1 μm pumped OPG stage of lower output power with a 515 nm pumped high-power OPA with moderate gain based on LBO, we have evaded all the above-mentioned limitations. Note that the conversion efficiency of the OPG is not very important, since the OPA can cope with limited signal pulse energy.

We investigated the OPG process further using the same numerical simulation model[10] as in Section 3. The model uses signal and idler inputs with numerically generated fluctuations to simulate the quantum noise, from which the OPG starts. The group velocity mismatch (GVM) automatically enters the model by using the Sellmeier equations of Ref. 24 to calculate the wavelength dependence of the refractive index. The measured OPG threshold is consistent with a nonlinearity of 8.2 pm/V in the simulations, which seems to be a reasonable value. Note that we are using a double-pass configuration, where pump and signal beams are reflected back into the crystal with a curved mirror. We found that a significantly higher conversion efficiency would in principle be possible for pumping further above threshold, but even if damage could be avoided in this regime, problems would arise from pulse breakup; for high pump powers, an additional pulse behind the main pulse is generated [dashed curve in Fig. 7(b), top graph]. This explains the roughly triangular shape of the autocorrelation (Fig. 5) for the highest output powers. The distorted pulse is a result of pump depletion, GVM, and (at the highest powers) backconversion. The temporal walk-off between signal and idler in a single pass through the OPG crystal is $\tau_{12} \approx 2.2$ ps, which is longer than the signal pulse. The generation of such a short signal pulse can be explained by temporal gain guiding by the short pump pulse. In the frequency domain, the large temporal walk-off corresponds to a phase-matching bandwidth $\Delta_v \approx 0.89/\tau_{12} \approx 400$ GHz, or $\sim$2.8 nm (where the constant 0.89 is explained in Ref. 28), which is

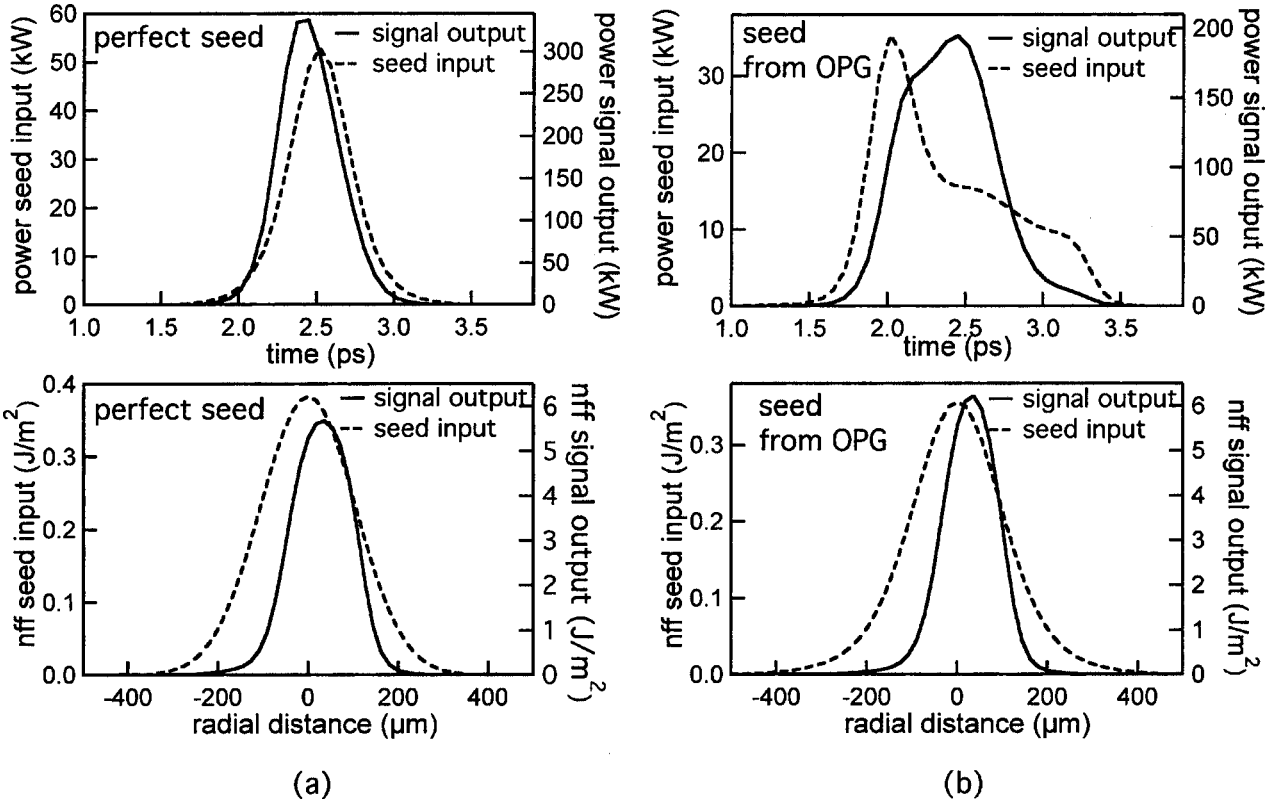

Fig. 7. Simulated instantaneous power (top) and near-field fluence (nff) in the critical plane (bottom) of the signal pulse before (dashed curve) and after (solid curve) the OPA for a perfect Gaussian seed beam (a) and a simulated OPG signal (b). The temporal profile of the distorted signal wave (b) is improved during the amplification process.

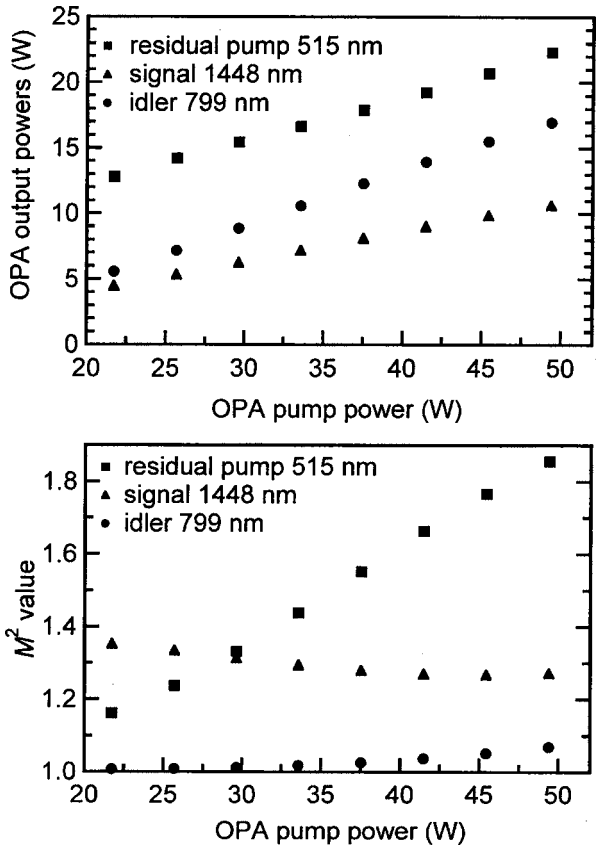

Fig. 8. Numerical simulations of the output power (top) and the beam quality (bottom) of the OPA as a function of the 515 nm pump power.

below the width of the signal spectrum. However, it must be noted that this definition of phase-matching bandwidth is meaningful only in a low-gain situation, where the signal amplitudes do not change much during the passage through the crystal. In a high-gain situation, the gain increases the tolerance to phase mismatch, and consequently the effective bandwidth.

We also used the numerical model to investigate how to optimize the performance of the OPA. The pump power at 515 nm is an important parameter for increasing the average power of the generated signal and idler waves. More pump power results in higher average power of both the signal and idler wave (Fig. 8, top graph). The beam quality of the signal wave is slightly improved for higher pump powers, whereas the beam quality of the residual pump is reduced owing to pump depletion (Fig. 8, bottom graph). The duration of the signal pulse decreases for increasing pump power, whereas pump depletion causes the transmitted pump-pulse duration to increase. As the saturation of the amplifier is significant, the output powers of signal and idler waves can be increased only slightly for higher seed average power.

It might seem beneficial to use a longer nonlinear crystal to improve the conversion efficiency, but owing to spatial walk-off the signal and idler powers are reduced for crystals longer than 10 mm, with the beam radii optimized for each crystal length. Better conversion could be obtained with a walk-off-compensated setup, in which a second crystal is oriented so as to compensate the walk-off from the first crystal. For example, with two 5 mm long LBO crystals in a walk-off-compensating setup instead of one 10 mm long crystal and with similar beam radii, the output powers of the signal and idler wave would be increased by 12% and 11%, respectively. However, higher conversion efficiency in the amplifier would result in an $\approx$8% increased M^2 value of the residual pump beam, owing to enhanced pump depletion. We did not use a shorter crystal, because the pump radius would then have to be smaller, and this would result in a higher pump intensity, increasing the risk of damage. In addition, stronger focusing in the 10 mm crystal also will not improve the efficiency, because of backconversion and spatial walk-off.

The amplification process smoothes the temporal pulse shape of the input signal pulse. Figure 7 shows a simulation of the temporal (Fig. 7, upper graphs) and spatial (Fig. 7, lower graphs) pulse shapes of the signal wave before (dashed curve) and after (solid curve) the OPA. In each simulation, we used the pump pulses at 515 nm originating from the SHG simulations. In the graphs on the left in Fig. 7 the seed pulse is assumed to have a perfect Gaussian spatial shape and a sech^2-shaped temporal profile, whereas in the graphs on the right the simulated signal output pulse from the OPG stage was used as seed pulse. The ideal pulse was chosen such that it had the same pulse energy and FWHM pulse duration as the simulated OPG signal pulse. The improvement of the temporal shape of the OPG signal pulse can clearly be seen. The signal output power of the OPA for an ideal seed beam would, however, be 10% higher than with the real temporally distorted beam from the OPG. The simulated optical spectrum [Fig. 9(b)] of the green output of the RGB system is quite similar to the measured optical spectrum [Fig. 9(c)]. The shoulders in the optical spectrum of the green output are caused by pump depletion, which imposes fast temporal variation on the pump beam, resulting in a broader spectrum. The simulated optical spectrum of the pump pulse entering the OPA stage does not yet show such shoulders [Fig. 9(a)]. The temporal walk-off between signal and idler in the OPA is only 175 fs, corresponding to a phase-matching bandwidth of 5 THz, so this does not limit the amplified spectrum.

Note that the power losses at the imperfect antireflection (AR) coatings (see above) are significant. Assuming that we could obtain LBO crystals with only 1% reflectiv-

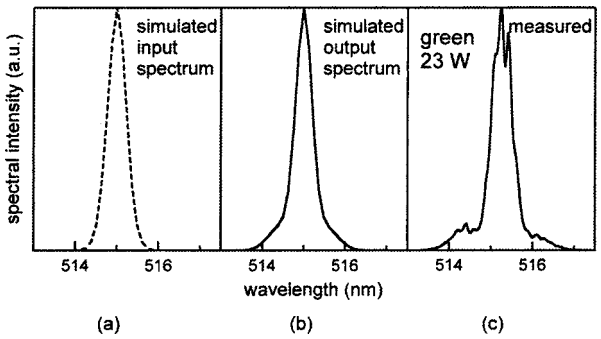

Fig. 9. Simulated optical spectrum of the pump beam at 515 nm (a) before and (b) after the amplification process in the OPA stage. (c) Measured optical spectrum of the 515 nm output of the RGB system (i.e., after the OPA). The shoulders in the optical spectrum are caused by pump depletion.

ity per surface for all wavelengths, simulations suggest that we would obtain 5% higher signal and 3% higher idler powers, namely, 9.6 W at 1448 nm and 14.5 W at 799 nm. Because the amount of signal and idler power is crucial for the following SFG stages, this would significantly increase the power of the generated red and blue beams.

5. SUM-FREQUENCY GENERATION

The wavelengths in the blue and the red spectral regions are generated in two subsequent SFG stages, where we mix the idler and signal waves from the OPA with the residual 22.6 W of 1030 nm light from the frequency doubler. The two SFG stages are based on two antireflection-coated LBO crystals, both critically phase matched at room temperature.

A. Experiment

The first SFG crystal is 10 mm long and mixes the 799 nm wave with the 1030 nm beam to generate the blue color at a wavelength of 450 nm (Fig. 10, right graph). The beam radii in the waist of the 1030 nm wave and the idler beam from the OPA are 205 μm. Phase matching in the first SFG stage is achieved with a Type I scheme (oo-e in the *XY* plane) with a phase-matching angle of $\varphi_{pm}=22.46°$ and a nonlinear coefficient of $d_{31}=0.85$ pm/V. The effective nonlinearity is 0.79 pm/V, and the walk-off angle of the blue beam is $\rho=12.9$ mrad. The AR coating of this LBO crystal again introduces relatively large reflection losses per surface of 1.2% at 1030 nm, 1.8% at 799 nm, 4% at 450 nm, and 3% at 1448 nm. The second SFG crystal is 15 mm long and generates the red beam at 603 nm (Fig. 10, left graph) by mixing the 1448 nm wave with the remaining 1030 nm light. Phase-matching in the LBO crystal is obtained with a Type I scheme (oo-e) with a rather small phase-matching angle $\varphi_{pm}=0.6°$, i.e., close to a noncritically phase-matched configuration, where the spatial walk-off is also small ($\rho=365$ μrad). The effective nonlinear coefficient is 0.85 pm/V. The beam radii of the 1030 nm input wave and the 1448 nm wave are both 105 μm in the waist. Because of the small spatial walk-off, we can use a tighter beam waist than in the first SFG stage. The reflection losses in the AR coating of this LBO crystal are 1.8% at 1030 nm, 1% at 603 nm, and 3.5% at 1448 nm. The peak intensity of the pump waves in those two LBO crystals is well below 1 GW/cm^2.

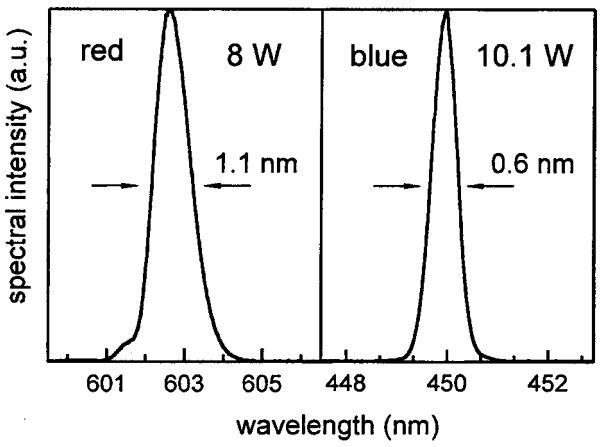

Fig. 10. Measured optical spectra of the 603 nm red and 450 nm blue outputs of the RGB system.

The generated blue beam at 450 nm has an average power of 10.1 W, and the beam quality is close to the diffraction limit, with $M^2=1.1$. The average power of the red beam at 603 nm is 8 W, again in a nearly diffraction-limited beam with $M^2=1.1$.

B. Simulation and Discussion

The following discussion is based on qualitative considerations, numerical simulations (based on the same numerical code as described above), and experimental experience, which is in good agreement with the simulations.

The order of the two SFG stages (first for blue, then for red) is dictated by phase-matching considerations: The SFG for generation of red light is close to being noncritically phase matched, i.e., with a very small spatial walk-off, which allows strong focusing and thus reasonable efficiency even with a low power in the residual 1030 nm light. On the other hand, the SFG stage for the generation of blue light has a large spatial walk-off, which prevents strong focusing and thus requires a higher 1030 nm input power. However, the available amount of pump power at 799 nm is smaller ($\approx$12 W incident) and thus more limiting than the power at 1030 nm. The beam quality of the 450 nm wave remains good for increasing pump powers of both pump wavelengths, and the beam quality of the residual 1030 nm pump wave degrades only slightly. In contrast to this, the effect of pump depletion for the 799 nm wave is much stronger. However, this is no problem since the residual of the 799 nm pump wave is not used. The pulse length of the blue beam is relatively insensitive to the amount of pump power at 799 and 1030 nm.

Simulations show that higher conversion efficiency to the blue beam could be obtained with a shorter crystal and smaller beam radii. For example, the use of a 5 mm long LBO crystal with a pump radius of 91 μm for the 1030 nm wave and a pump radius of 103 μm for the 799 nm wave would increase the amount of blue power by 20%, mainly because the influence of the GVM is reduced. Note that because of the short blue wavelength the GVM is much larger in the first SFG stage compared with that in the infrared conversion stages. For a length of 10 mm, the total temporal walk-off between 1030 nm pump and the blue wave is 944 fs, which is almost the width of the pump pulse, which is simulated to be 1180 fs. The effect of the spatial walk-off, on the other hand, is not reduced for a shorter crystal, because stronger focusing is required. The simulations show signs of partial backconversion to the residual pump waves on the beam axis, but the beam quality of the generated blue beam is not yet negatively influenced.

Simulations for the experimental situation with improved AR coatings (with an assumed reflectivity of 1% per surface for all wavelengths) result in 26% higher power of the blue beam. With a shorter (4 mm long) crystal and optimized mode areas, even 51% higher average power at 450 nm could be obtained. The blue average power would in this case be 18.9 W with a still good M^2 value of 1.15.

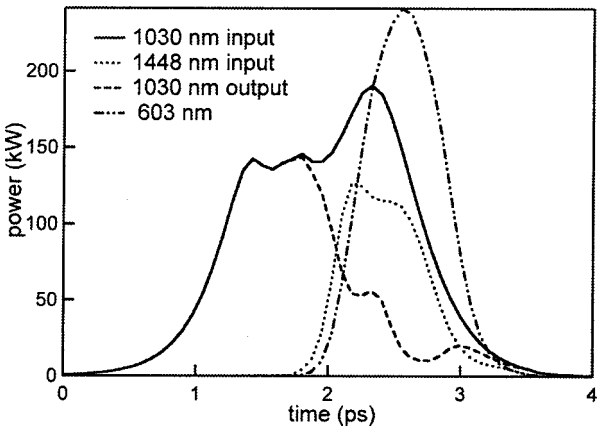

Fig. 11. Simulated input (solid curve) and output (dashed curve) temporal pulse shape of the 1030 nm wave in the red SFG stage. The dotted curve corresponds to the temporal pulse shape of the input 1448 nm wave, and the dashed–dotted curve corresponds to the generated red beam at 603 nm.

We now discuss the second SFG stage, i.e., the one for the generation of red light. Increasing the power of either pump beam separately does not increase the red output significantly. This indicates that the SFG process is strongly saturated, in spite of about 10 W of transmitted power at 1030 nm. The reason for this is that the 1030 nm pulse after the blue SFG stage is much longer than the 1448 nm pulse (see Fig. 11), so they don't fully overlap. Note that the temporal walk-off between 1030 nm and 1448 nm is only 13 fs in 15 mm, so that it is not possible to obtain a high conversion efficiency. On the other hand, the effect of spatial walk-off is negligible in this stage.

Assuming better AR coatings with 1% reflection loss per surface for all LBO crystals and mode radii optimized for this situation, we would expect from simulations to obtain $\approx$10 W instead of 8.1 W in the red beam. Here, the simulated signal power from the OPA (also with optimized AR coatings) is 9.3 W, and the remaining power at 1030 nm for the red SFG stage is 15.2 W. The LBO crystal would have to be 12 mm long, and the pump radii required are 174 μm for 1030 and 1448 nm.

As the second SFG stage suffers from the temporal distortion of the 1030 nm light in the first SFG stage, one might consider using the two SFG stages in a parallel setup; i.e., with a beam splitter, to provide each SFG stage with a fraction of the total power of the original 1030 nm beam. Simulations showed that similar output powers in the red and blue could be obtained with such a configuration but with somewhat-deteriorated beam quality of the blue beam, because stronger focusing is required in the blue SFG stage, so that the spatial walk-off becomes more important. Moreover, one would need an additional adjustable delay line.

The wavelength of the red output is a bit shorter than that of the desired red ($\geq$620 nm) for an RGB laser source. This could in principle be solved with a new PPSLT crystal with a poling period for a longer signal wavelength. One constraint imposed by our system is that the difference in photon energy between the blue and green colors equals the one between the green and red colors. For example, one could choose a red wavelength of 620 nm in combination with a blue wavelength of 440 nm by designing the poling period of the OPG for a signal wavelength of 1560 nm instead of 1448 nm. The other constraint in the OPG is the effect of the GVM that will (as numerical simulations show) deteriorate the conversion process if the signal wavelength is shifted to 1560 nm. For the original signal wavelength of 1448 nm, the group index of the pump wave lies between the indices of the signal and idler waves. This situation has been shown[29] to be ideal for the conversion efficiency. In contrast, a situation with signal and idler waves both propagating faster or slower than the pump wave will result in stronger saturation of the parametric gain. This exactly will be the case for a signal wavelength shifted to $>$1520 nm, as then the group index of the pump wave will be higher than the ones of signal and idler. This behavior of the group indexes is similar in other nonlinear materials such as KTP ($KTiOPO_4$), RTA ($RbTiOAsO_4$), or LBO. Simulations predict that we could get the required performance from the OPG for a signal wavelength of up to $\approx$1510 nm. However, for an average signal power of 1.53 W in this situation, we would already require a higher pump power of 9.5 W, as the parametric gain is reduced owing to the enhanced GVM. With a signal wavelength of 1510 nm, we would obtain a red wavelength of 612 nm (still a bit short for displays) and a blue wavelength at 444 nm. It turns out that a laser wavelength of 1064 nm would actually lead to more favorable group velocities in the OPG stage, even for optimum display wavelengths. However, our system requires relatively short pulses, as we are using critical phase matching in several conversion stages, and so far there is no 1064 nm laser generating such pulses with sufficient peak power.

6. DISCUSSION AND OUTLOOK

We have analyzed a powerful RGB laser system that in our experiments delivered 8 W at 603 nm (red), 23 W at 515 nm (green), and 10.1 W at 450 nm (blue). The system is based on a passively mode-locked Yb:YAG thin disk laser. A first key point for optimum performance of the chosen configuration of nonlinear conversion stages is that our laser produces subpicosecond pulses and thus a very high peak power that allows the use of LBO crystals in critically phase-matched schemes for nonlinear conversion stages operating at room temperature. With, for example, ten-times-longer pulses from the laser, one would require noncritically phase-matched conversion stages to achieve efficient conversion, which would then require several crystal ovens operated at elevated temperatures. A high average power at 515 nm is crucial for the amount of power of signal and idler waves generated in the OPA stage. At the same time, sufficient residual 1030 nm light with a good beam quality from the frequency doubler is required for the further conversion stages. An OPG stage based on PPSLT allows the generation of stable 1.6 W signal power at 1.5 μm. With the recently demonstrated room-temperature OPG based on MgO-doped SLT, this last temperature-stabilized crystal can be replaced by an OPG operated at room temperature with the same performance. The power of the 799 nm pump light is crucial for a good conversion in the blue SFG stage, which is limited

by GVM and spatial walk-off. The efficiency of the red SFG stage is limited by the temporal distortion of 1030 nm light in the blue SFG stage. Because of this distortion and the available input powers, the red SFG stage works best if the blue SFG stage is not optimized for maximum blue output power. The detailed analysis showed that the overall performance of our system could not have been significantly improved with modified crystal lengths or focusing conditions, but better antireflection coatings could increase the output powers significantly. Note that the fabrication of these coatings is not trivial, particularly for the first (blue) SFG stage, where four wavelengths are involved. Assuming a reflectivity of the AR coatings of 1% per surface for all wavelengths, simulations predict the following performance (using the same powers from the laser, the frequency doubler and the OPG as in the experiment): The output of the OPA could be improved to 9.6 W of signal and 14.5 W of idler power. The OPA crystal length in this simulation was unchanged (10 mm), and the pump radii were 125 μm at 515 nm and 175 μm at 1448 nm. With beam radii of 330 μm at 1030 nm and 312 μm at 799 nm in the first SFG stage, a blue beam with an average power of 11.2 W at 450 nm with good beam quality could be generated. The crystal length in this simulation was again unchanged (10 mm), and the focusing was weaker than for optimum blue light generation in order to obtain better performance in the following red stage. After the blue SFG stage, 17.2 W of residual 1030 nm light would be left as a first pump wave for the red SFG crystal. Finally, using a crystal with 12 mm length in the red SFG stage, a pump beam radius of 168 μm at 1030 nm, and 173 μm for the signal wave from the OPA, a red beam at 603 nm with an average power of 12 W could be generated.

In an optimized configuration, the RGB laser system could generate a significantly higher total power of D65 (ISO 10526:1999/CIE S005/E-1998 standard) white light, which is an important parameter for an RGB laser source. With the above-mentioned powers and the wavelengths as generated in the experiment (603, 515, and 450 nm), the total D65 white-light power would be 37.5 W (12 W red, 16 W green, and 9.5 W blue), corresponding to 11 265 lm. The total conversion efficiency from the laser wavelength to D65 would be 47.5%, and the total infrared to visible conversion efficiency would be 53%. The numerical analysis of the OPG stage showed that it is difficult to shift the signal wavelength to the desired value of 1560 nm in order to generate a red color at 620 nm. It turned out, however, that a signal wavelength of 1510 nm in the OPG should be possible, at least increasing the red wavelength by 10 nm to 612 nm. With improved wavelengths of 612, 515, and 445 nm, one could obtain 37.4 W of D65 power (12 W red, 16.6 W green, and 8.8 W blue), assuming unchanged conversion efficiencies. The amount of D65 white light with optimized wavelength would be somewhat reduced, but the color gamut spanned by those optimized wavelengths would be larger. A laser wavelength of 1064 nm would actually make it easier to generate the optimum wavelengths for the display with optimum conversion efficiency, because the group velocities in the OPG stage would be more favorable for efficient conversion. However, there currently exists no laser material at 1064 nm that is suitable for the generation of femtosecond pulses with high average output power.

In conclusion, the analyzed RGB system is unprecedented in terms of generated average powers in the colors as well as in its simplicity and practicability. One single laser oscillator without any amplifier stages provides the entire pump power of the system. The system does not require any synchronized cavities and can be realized with room-temperature operation of all of the nonlinear crystals.[11] The approach with separated parametric generation and amplification allows generating the required high average power beams for the generation of the red and the blue colors. Numerical simulations showed that improved AR coatings should allow achieving even better performance, with excellent conversion efficiency from infrared to D65, even though it is predicted that reaching a longer wavelength for the red output, as is desirable for displays, might be difficult. The previous point, among others, demonstrates that a careful investigation based on numerical simulations can greatly facilitate the physical understanding of device operation, optimization of device performance, and identification of limitations.

REFERENCES

1. S. R. Kubota, "The grating light valve projector," Opt. Photonics News **9**, 50–53 (2002).
2. O. Solgaard, F. Sandejas, and D. M. Bloom, "Deformable grating optical modulator," Opt. Lett. **17**, 688–690 (1992).
3. R. Wallenstein, "Advanced solid state sources for high power visible light generation," in *Conference on Lasers and Electro-Optics*, Vol. 56 of OSA Trends in Optics and Photonics Series (Optical Society of America, 2001), paper CThC3, p. 389.
4. D. Lee and P. F. Moulton, "High-efficiency, high-power, OPO-based RGB source," in *Conference on Lasers and Electro-Optics*, Vol. 56 of OSA Trends in Optics and Photonics Series (Optical Society of America, 2001), paper CThJ2, p. 424.
5. J. Aus der Au, G. J. Spühler, T. Südmeyer, R. Paschotta, R. Hövel, M. Moser, S. Erhard, M. Karszewski, A. Giesen, and U. Keller, "16.2 W average power from a diode-pumped femtosecond Yb:YAG thin disk laser," Opt. Lett. **25**, 859–861 (2000).
6. E. Innerhofer, T. Südmeyer, F. Brunner, R. Häring, A. Aschwanden, R. Paschotta, U. Keller, C. Hönninger, and M. Kumkar, "60 W average power in 810-fs pulses from a thin-disk Yb:YAG laser," Opt. Lett. **28**, 367–369 (2003).
7. F. Brunner, T. Südmeyer, E. Innerhofer, R. Paschotta, F. Morier-Genoud, J. Gao, K. Contag, A. Giesen, V. E. Kisel, V. G. Shcherbitsky, N. V. Kuleshov, and U. Keller, "240-fs pulses with 22-W average power from a mode-locked thin-disk Yb:$KY(WO_4)_2$ laser," Opt. Lett. **27**, 1162–1164 (2002).
8. R. Wallenstein, "Process and apparatus for generation at least three laser beams of different wavelength for the display of color video pictures," U.S. Patent 5,828,424 (1998).
9. F. Brunner, E. Innerhofer, S. V. Marchese, T. Südmeyer, R. Paschotta, T. Usami, H. Ito, S. Kurimura, K. Kitamura, G. Arisholm, and U. Keller, "Powerful red-green-blue laser source pumped with a mode-locked thin disk laser," Opt. Lett. **29**, 1921–1923 (2004).
10. G. Arisholm, "Quantum noise initiation and macroscopic fluctuations in optical parametric oscillators," J. Opt. Soc. Am. B **16**, 117–127 (1999).
11. S. V. Marchese, E. Innerhofer, R. Paschotta, S. Kurimura, K. Kitamura, G. Arisholm, and U. Keller, "Room temperature femtosecond optical parametric generation in

MgO-doped stoichiometric $LiTaO_3$," to appear in Appl. Phys. B (to be published).
12. A. Giesen, H. Hügel, A. Voss, K. Wittig, U. Brauch, and H. Opower, "Scalable concept for diode-pumped high-power solid-state lasers," Appl. Phys. B **58**, 363–372 (1994).
13. U. Keller, D. A. B. Miller, G. D. Boyd, T. H. Chiu, J. F. Ferguson, and M. T. Asom, "Solid-state low-loss interactivity saturable absorber for Nd:YLF lasers: an antiresonant semiconductor Fabry–Perot saturable absorber," Opt. Lett. **17**, 505–507 (1992).
14. U. Keller, K. J. Weingarten, F. X. Kärtner, D. Kopf, B. Braun, I. D. Jung, R. Fluck, C. Hönninger, N. Matuschek, and J. Aus der Au, "Semiconductor saturable absorber mirrors (SESAMs) for femtosecond to nanosecond pulse generation in solid-state lasers," IEEE J. Sel. Top. Quantum Electron. **2**, 435–453 (1996).
15. F. X. Kärtner and U. Keller, "Stabilization of soliton-like pulses with a slow saturable absorber," Opt. Lett. **20**, 16–18 (1995).
16. F. X. Kärtner, I. D. Jung, and U. Keller, "Soliton modelocking with saturable absorbers," IEEE J. Sel. Top. Quantum Electron. **2**, 540–556 (1996).
17. F. Gires and P. Tournois, "Interferometer utilisable pour la compression d'impulsions luminousness modules en frequence," C. R. Acad. Sci. Paris **258**, 6112–6115 (1964).
18. S. Lin, Z. Sun, B. Wu, and C. Chen, "The nonlinear optical characteristics of a LiB_3O_5 crystal," J. Appl. Phys. **67**, 634–638 (1990).
19. S. P. Velsko, M. Webb, L. Davis, and C. Huang, "Phase-matched harmonic generation in lithium triborate (LBO)," IEEE J. Quantum Electron. **27**, 2182–2192 (1991).
20. D. A. Roberts, "Simplified characterization of uniaxial and biaxial nonlinear optical crystals: a plea for standardization of nomenclature and conventions," IEEE J. Quantum Electron. **28**, 2057–2074 (1992).
21. G. Arisholm, R. Paschotta, and T. Südmeyer, "Limits to the power scalability of high-gain optical parametric amplifiers," J. Opt. Soc. Am. B **21**, 578–590 (2004).
22. J. Biegert and J.-C. Diels, "Compression of pulses of a few optical cycles through harmonic generation," J. Opt. Soc. Am. B **18**, 1218–1226 (2001).
23. K. Kitamura, Y. Furukawa, K. Niwa, V. Gopalan, and T. E. Mitchell, "Crystal growth and low coercive field 180° domain switching characteristics of stoichiometric $LiTaO_3$," Appl. Phys. Lett. **73**, 3073–3075 (1998).
24. A. Bruner, D. Eger, M. B. Oron, P. Blau, M. Katz, and S. Ruschin, "Temperature-dependent Sellmeier equation for the refractive index of stoichiometric lithium tantalate," Opt. Lett. **28**, 194–196 (2003).
25. T. Südmeyer, J. Aus der Au, R. Paschotta, U. Keller, P. G. R. Smith, G. W. Ross, and D. C. Hanna, "Novel ultrafast parametric systems: high repetition rate single-pass OPG and fibre-feedback OPO," J. Phys. D **34**, 2433–2439 (2001).
26. T. Südmeyer, F. Brunner, R. Paschotta, U. Keller, T. Usami, H. Ito, M. Nakamura, and K. Kitamura, "Femtosecond optical parametric generation (OPG) in periodically poled stoichiometric $LiTaO_3$ with >1 W average power," in *Conference on Laser and Electro-Optics*, Vol. 73 of OSA Trends in Optics and Photonics Series (Optical Society of America, 2002), paper CTuO4, p. 260.
27. B. Köhler, U. Bäder, A. Nebel, J.-P. Meyn, and R. Wallenstein, "A 9.5-W 82-MHz-repetition-rate picosecond optical parametric generator with cw diode laser injection seeding," Appl. Phys. B **75**, 31–34 (2002).
28. G. Arisholm, G. Rustad, and K. Stenersen, "Importance of pump-beam group velocity for backconversion in optical parametric oscillators," J. Opt. Soc. Am. B **18**, 1882–1890 (2001).
29. R. Danielius, A. Piskarskas, A. Stabinis, G. P. Banfi, P. Di Trapani, and R. Righini, "Traveling-wave parametric generation of widely tunable, highly coherent femtosecond light pulses," J. Opt. Soc. Am. B **10**, 2222–2232 (1993).